CrossMark

Formation Regularities of Plasmonic Silver Nanostructures on Porous Silicon for Effective Surface-Enhanced Raman Scattering

Hanna V. Bandarenka[1*], Kseniya V. Girel[1], Vitaly P. Bondarenko[1], Inna A. Khodasevich[2], Andrei Yu. Panarin[2] and Sergei N. Terekhov[2]

Abstract

Plasmonic nanostructures demonstrating an activity in the surface-enhanced Raman scattering (SERS) spectroscopy have been fabricated by an immersion deposition of silver nanoparticles from silver salt solution on mesoporous silicon (meso-PS). The SERS signal intensity has been found to follow the periodical repacking of the silver nanoparticles, which grow according to the Volmer–Weber mechanism. The ratio of silver salt concentration and immersion time substantially manages the SERS intensity. It has been established that optimal conditions of nanostructured silver layers formation for a maximal Raman enhancement can be chosen taking into account a special parameter called effective time: a product of the silver salt concentration on the immersion deposition time. The detection limit for porphyrin molecules CuTMPyP4 adsorbed on the silvered PS has been evaluated as 10^{-11} M.

Keywords: Porous silicon, Silver nanoparticles, Immersion deposition, Surface-enhanced Raman scattering, Detection limit

Background

Surface-enhanced Raman scattering (SERS) spectroscopy is widely recognized as a label-free high-sensitive method for applications in analytical chemistry [1, 2], biomedicine [3–5], and various sensor devices [6–9]. SERS is observed for analyte molecules adsorbed on the noble metal surfaces with nanoscale roughness, so-called SERS-active substrates [10, 11]. An enormous level of Raman signal in SERS is mainly attributed to the strong enhancement of the local electromagnetic field near the metallic nanostructures or junctions between them [12, 13], resulted from the excitation of surface plasmon resonance (SPR)—the coherent oscillations of electrons at metal-dielectric interfaces [14, 15].

A fabrication of novel effective and inexpensive plasmonic nanostructures with well-defined nanoscale

geometry, which demonstrate strong, reproducible, and stable Raman signal, is an important current challenge to make SERS spectroscopy a routine practical method for a wider range of applications. Accordingly, a number of different methods have been developed for the formation of plasmonic materials suitable for SERS, as might be evidenced from the recent reviews [16, 17].

Metallic nanoparticles (NPs) of different size and shape synthesized through ordinary wet chemistry and immobilized on solid substrates by various techniques have been thoroughly studied and extensively used in SERS experiments [10, 18]. There are many ways of immobilization of the metallic NPs on the solid substrates including chemical attachment with the use of bifunctional molecules, self-assembly based on electrostatic attraction, using capillary force as a driving mechanism for deposition, and chemical and photochemical growth. However, the abovementioned methods often cause dispersion and aggregation of the metallic NPs making difficult to provide enough reproducibility of the characteristics of SERS-active substrates in practice. To overcome the aforementioned limit, modern

* Correspondence: h.bandarenka@bsuir.by
[1]Laboratory of Materials and Structures of Nanoelectronics, Belarusian State University of Informatics and Radioelectronics, 6 Brovka st., Minsk 220013, Belarus
Full list of author information is available at the end of the article

Bandarenka *et al. Nanoscale Research Letters* (2016) 11:262

Page 2 of 11

nanofabrication approaches such as electron-beam and nanosphere lithography, Langmuir–Blodgett technique and self-ordering method have been proposed [19–21]. However, these technologies are rather high cost and require substantial experience of an operator.

In terms of simplicity and cost-effectiveness, a lithography-free approach based on the using porous templates is one of the most promising ways to fabricate plasmonic nanostructures with controlled geometry, long-range ordering, and well-defined size and shape. Recently, it has been shown that metalized porous silicon (PS) demonstrates promising features for effective SERS. PS is known for its exceptional properties such as the extremely high effective surface area, large adsorption capacity, photo- and electroluminescence, and biocompatibility [22, 23]. Metallic coatings can be formed on the PS template via various techniques: thermal decomposition of metal salt in an oxidized PS [24, 25]; metal-assisted wet etching and sputtering processes [26]; physical vapor deposition [27]; inject printing synthesis [28]; and immersion plating of metals within the pores of PS [29–31]. The most significant advantage of the PS template is a possibility to vary and precisely control structural parameters of the porous layers, thus affecting the morphology of such plasmonic metal nanostructures.

The immersion plating occupies a special place among the other metal deposition techniques as this method does not require vacuum equipment, energy supply or special reducing agents: it is carried out due to redox reactions between atoms of a substrate and metal ions. In case of Si-based substrates, solutions containing ions of metals with positive redox potential (Cu and noble metals) have to be used to provide the immersion deposition [32]. By nowadays, several reports have described immersion deposition of gold [33], copper [34], and silver [35–40] on PS at different conditions to form SERS-active substrates. Silver deposits have been mainly used to form SERS-active substrates based on PS due to the strongest plasmonic properties of this metal [41]. A dependence of the Ag nanostructure morphology and SERS activity on various PS parameters (thickness, porosity, and pore diameter) and Ag deposition regimes (an immersion time, a temperature, and a concentration of the solution reagents) have been investigated [38].

In the issue of aforementioned works, the properties of Ag nanostructures fabricating at the same immersion solution temperature on the identical PS samples have been found to depend on the following main factors: (i) the concentration of Ag ions and (ii) the Ag deposition duration. Nevertheless, these two factors have been hardly combined for different cases of the SERS-active substrates formation.

Giorgis' group has carefully studied a morphology of Ag samples synthesized by the PS immersion in a 1–10 mM $AgNO_3$ aqueous solution for 0.5–10 min at a temperature

of 5–50 °C [30, 37]. The strongest Raman enhancement has been observed for the case of an excitation wavelength matching with the SPR band of the Ag/PS substrates. Recently, it has been reported detection of crystal violet with Ag nanostructures formed by the PS immersion in a 10 mM $AgNO_3$ aqueous solution for a period ranging from 15 to 120 s [36]. The most intensive SERS signal has been typical for the substrate prepared by the 30s immersion plating. Zeiri et al. [35] have studied the silver immersion deposition on PS in the $AgNO_3$ solutions, which contain different concentration of Ag^+ ions (from 1 to 500 mM). The deposition time was 30 min. The largest SERS activity was reached for the substrate formed with the 50 mM Ag^+ solution. We have investigated SERS-active substrates prepared on the PS templates based on *p*- and *n*-type silicon wafers by the immersion deposition for 1 to 30 min in 1, 10, and 100 mM $AgNO_3$ solutions [31, 38]. The best SERS results for rhodamine 6G probing molecule have been obtained for the samples formed by the Ag deposition in a 10 mM $AgNO_3$ aqueous solution during 10–15 min and 5 min for the PS samples based on *p*- and *n*-type silicon wafers, respectively.

An ultimate goal of the described works was to reveal correlation between the concentration of the Ag salt and the deposition time to find optimal fabrication conditions for the most effective SERS. Obviously, an increase of the Ag^+ concentration in the solution leads to the Ag deposition fastening. However, the rapid process makes difficult careful control of the morphology of the Ag structures, which can coalesce into continuous film or large aggregates not favorable for SERS activity. On the other hand, a highly diluted Ag salt solution results in a very slow silver deposition. Moreover, H^+ ions in aqueous solutions can compete with Ag^+ ions in the oxidation of the silicon atoms. In this case, the PS surface will be covered with silicon oxide before formation of sufficient amount of silver deposit. Therefore, the question arises on the choice of proper conditions of the Ag immersion deposition on PS, i.e., relation between the Ag salt concentration and the immersion duration.

Herein, we report a systematic study of the Ag nanostructures formed by the immersion technique on the PS surface. We used the highly doped n^+-type silicon wafers as it allows fabrication of the mesoporous silicon (meso-PS) composed of ordered vertical pores. Such material is a perfect template for the metallic deposit formation with required spatial location. The appropriate Ag nanostructures were produced in three solutions of different $AgNO_3$ concentration. The deposition duration was varied in the wide range from a few to 200 min. SERS efficiency of the Ag/PS substrates was evaluated using water-soluble cationic porphyrin CuTMPyP4. Based on the analysis of the regularities of the Ag nanostructures growth and corresponding kinetics of SERS-signal intensity change, we revealed a parameter crucial for the formation of the SERS-active substrates,

Bandarenka *et al. Nanoscale Research Letters* (2016) 11:262

Page 3 of 11

which can be defined as a product of the Ag salt concentration by the immersion deposition time.

Methods

Antimony doped 100 mm monocrystalline Si wafers of (100) orientation, and 0.01 Ω cm resistivity were used as an initial substrates. A chemical cleaning of the Si wafers was performed for 10 min in a hot (75 °C) solution of NH_4OH, H_2O_2, and H_2O mixed in a volume ratio of 1:1:4. The Si wafers rinsing with a deionized water and drying in a centrifuge followed the cleaning. Then the Si wafers were cut into a number of rectangular samples with an area of 9 cm^2. Some of the samples were used to deposit Ag on the surface of the original monocrystalline Si for a comparison of the immersion process on both the Si and PS templates. Just before the PS formation or the Ag immersion deposition, each Si sample was dipped in a diluted HF (5 %) for 30 s to remove a native oxide. Immediately after the native oxide removal, the Si sample was placed in an electrolytic cell made of polytetrafluoroethylene. An active opening of the cell had a round shape and an area of 3 cm^2. A highly pure graphite disk was used as a contact electrode to a backside of the samples during the electrochemical treatment. A platinum spiral wire was used as a cathode electrode. The PS layers were formed by an electrochemical anodization of the Si samples in a solution of HF (45 %), H_2O, and C_3H_7OH mixed in a 1:3:1 volume ratio according to the procedure described elsewhere [42]. The anodization was performed at a current density of 100 mA/cm^2 for 85 s. Such anodizing regimes provided fabrication of uniform PS layers of a 5-μm thickness and an average pore diameter of 60 nm at the top of PS layer. The resulting PS sample was kept for 30 min in C_3H_7OH to remove the products of the electrochemical process from the pores.

The Ag deposition on the samples of Si and PS was carried out by the immersion plating in 1, 3, and 10 mM $AgNO_3$ aqueous solutions with an ethanol additive. The immersion continued for 5–280 min. The Ag-coated samples were thoroughly rinsed with the deionized water and ethanol and then dried in the air.

The SERS activity of the experimental samples was studied using a cationic Cu(II)-tetrakis(4-*N*-methylpyridyl) porphyrin (CuTMpyP4) which was synthesized according to standard procedures by Dr. V.L. Malinovskii (Bogatsky Physico-Chemical Institute, Odessa, Ukraine). The samples for the SERS measurements were prepared by an incubation of the Ag-coated PS in the analyte aqueous solution of various molar concentrations (10^{-6}–10^{-12} M) during 2 h. Prior to impregnation with the analyte solution, the Ag-coated substrates were rinsed with a solution of HCl and H_2O mixed in 1:99 volume ratio. It provided an elimination of contaminants adsorbed on a high surface area of the Ag deposit that results in a strong SERS background.

All abovementioned procedures were carried out at the room temperature. The potentiostat/galvanostat AUTOLAB PGSTAT302n (The Netherlands) was used to conduct electrochemical processes.

Gravimetric method was applied to determine the porosity of PS. Mass measurements were performed with a Sartorius CP225D micro/analytical electronic balance (Germany). The instrumental mass error was 10 μg. The morphology of the samples was studied by the scanning electron microscopy (SEM; Hitachi S-4800, Japan) with 1 nm resolution. The phase composition of the samples was determined by X-ray diffraction (XRD) using CuKα radiation (X-ray wavelength λ = 0.15406 nm).

The electronic absorption spectra of the CuTMpyP4 solutions were measured with a Cary 500 Scan spectrophotometer (Varian, USA) in 10 × 10 mm quartz cells. Reflectance spectra of the Ag-coated samples were measured with the spectrophotometer MC 122 (Proscan Special Instruments, Belarus) in the range of 200 to 1000 nm. SERS spectra were recorded with 90° scattering geometry by using Solar TII DM160-MS3504I spectrometer equipped with a CCD detector SPEC10:256E (Roper Scientific, USA) cooled down to 153 K with liquid nitrogen. Excitation at 441.6 nm was provided by He–Cd laser (Liconix, USA). The cylindrical lens was used to stretch out the spot to 5 mm in length. All measurements were made at the room temperature.

Results and Discussions

Structure of the Ag-Coated PS Samples

During the process of immersion deposition of silver, meso-PS plays not only a role of the template defining a shape, dimensions, and spatial location of the Ag nanostructures. It also acts as a source of Ag nucleation centers and electrons for the reduction of Ag^+ ions that allows avoiding the use of special reducing agents and surface activators, which can be incorporated in the Ag deposit, thus resulting in an undesirable noise in SERS spectra. The Ag film formation on the PS surface proceeds in accordance with the Volmer–Weber mechanism [43] and the model proposed by Ogata's group [44]. PS acts as a mild reducing agent, which can spontaneously reduce metallic ions which have positive reduction potentials with respect to hydrogen. We checked the possibility of Ag film formation on the monocrystalline Si wafer by the immersion deposition. Despite a small amount of the Ag deposit was observed on the Si surface, no SERS activity was revealed for those samples. It is explained as follows: an exposure of the monocrystalline Si in the Ag salt aqueous solutions causes simultaneously with growth of Ag nanoparticles and a continuous layer of SiO_2. The oxide layer prevents contact of $AgNO_3$ with the Si atoms resulting in the limitation retardation of the metal

reduction. Below, it will be shown that an extremely developed specific surface area of PS and its open structure provide formation of an enough amount of the nanostructured Ag deposit favorable for the high efficient SERS activity.

Figure 1 presents the X-ray diffraction pattern of the PS sample after Ag immersion deposition from the 1 mM $AgNO_3$ solution for 120 min. It can be seen that Ag deposit on the PS sample has a polycrystalline nature because the pattern contains characteristic peaks, which give an evidence of the cubic cell Ag crystals with orientations (111), (200), (220), and (311). The same view of the XRD pattern was typical for all Ag-coated PS samples distinguishing just in intensity of the characteristic peaks, which depended on the $AgNO_3$ concentration and immersion time.

Using SEM analysis we revealed that in the regimes of the immersion, Ag deposit covers the PS top surface as the layer of particles. On the other hand, the inner surface of pore walls remains almost free of Ag NPs. We suggest that diffusion limitations in the pore channels prevent Ag^+ ions penetration and deposition inside porous layer.

As it was mentioned in the "Background" section, the morphology of Ag coating on the PS surface strongly depends on the silver nitrate concentration and on the immersion deposition time. Aiming to explore regularities of the Ag nanostructures growth on PS and their correlation with an enhancement of the SERS signal, we prepared the Ag/PS samples using different combinations of these two parameters. Below three cases of the Ag deposit morphology resulted from the deposition in different solutions are considered: (i) 1 mM; (ii) 3 mM

as a medium point within minimum and maximum concentration, and (iii) 10 mM.

Morphology of the Ag/PS Samples Formed in the 1 mM $AgNO_3$ Solution

Figure 2 shows SEM images of the top of the PS samples after immersion in 1 mM $AgNO_3$ solution, which demonstrates typical morphology changes of the Ag coating during deposition process. Below the SEM images, corresponding size distribution histograms of Ag NPs are presented. As seen from Fig. 2, at the initial stage of deposition, the PS surface was slightly covered with the separated Ag NPs (islands) with diameters of a few to several tens of nanometers (Fig. 2a). The distance between Ag NPs varies from 150 to 500 nm. Further deposition of Ag led to the multiplication of the particles and increase of their dimensions resulted in the formation of Ag agglomerates. Most of Ag agglomerates are connected or located extremely close to each other (Fig. 2b) bearing the structure similar to a quasi-continuous film. We suggest that the Ag coating grew according to the Volmer–Weber mechanism [43] because formation of the Ag film followed by the growth of the initial Ag islands (Fig. 2a, b). Prolongation of the immersion deposition time up to 180 min caused the coalescence of the Ag agglomerates into large particles of an average diameter varied in the range of 400–800 nm (Fig. 2c). The coalescence takes a place due to an increase of the mutual attraction between Ag atoms during continuous deposition. This effect is typical for the Volmer–Weber mechanism as well. At the same time, disconnection of the Ag agglomerates at the coalescence process allowed reopening the PS surface for a growth of new Ag NPs. This effect is in correspondence with the model of the
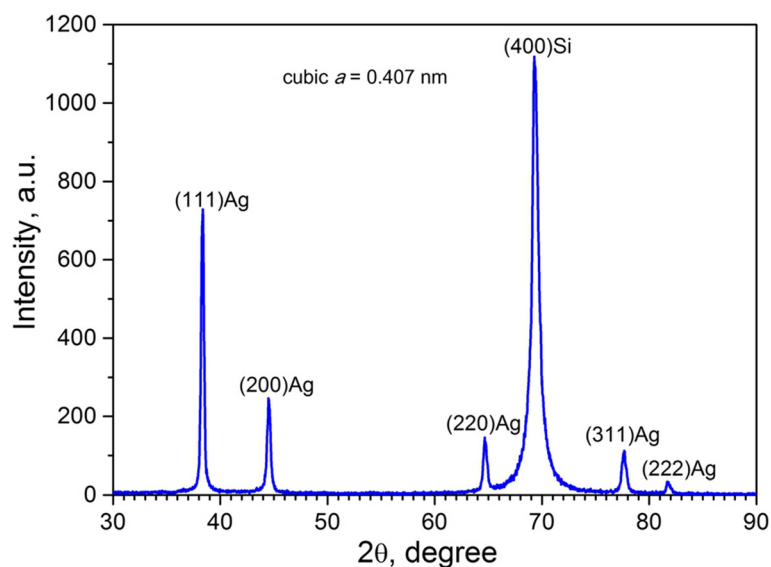

Fig. 1 X-ray diffraction pattern of the Ag-coated PS. The Ag immersion deposition was carried out from the 1 mM $AgNO_3$ solution for 120 min

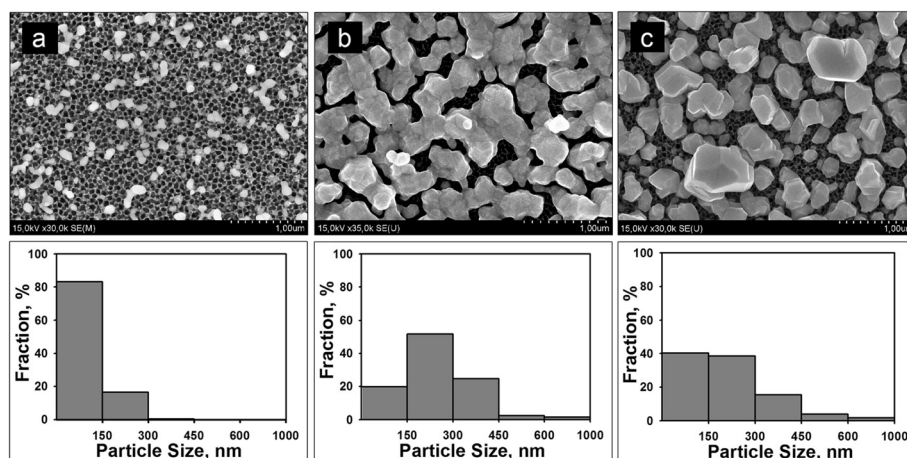Bandarenka *et al. Nanoscale Research Letters* (2016) 11:262

Page 5 of 11

Fig. 2 SEM top views of the PS samples after the immersion into 1 mM AgNO$_3$ solution. Ag was deposited for **a** 15, **b** 120, and **c** 180 min. Below corresponding histograms of Ag NPs size distribution are presented. The histograms are normalized with respect to the total number of Ag NPs

immersion deposition of metals on PS described earlier [32]. The analysis of the histograms reveals that size of Ag NPs for all the samples is favorable for the SERS effect (10–150 nm). Additionally, since the SERS activity is also affected by the mutual position of Ag NPs, i.e., the distance between them, the greatest intensity of the Raman signal is expected for the tightly packed but not connected Ag NPs. In our case, the distance between Ag NPs periodically varies depending on the deposition time. Based on this fact, one can suppose that the quasi-continuous Ag film (Fig. 2b) will demonstrate the maximum SERS performance, because the closely packed Ag agglomerates promote an abundance of vacancies for so-called hot spots, i.e., the scattering cross section of the analyte molecules should drastically increase.

Morphology of the Ag/PS Samples Formed in the 3 and 10 mM AgNO$_3$ Solutions

The similar mechanism of the Ag immersion deposition on PS was observed for 3 and 10 mM AgNO$_3$ concentrations. However, the duration of each deposition stage went into decline upon the increase of the Ag$^+$ ions number.

Figures 3 and 4 show SEM images of the top of PS sample views after immersion in the 3 and 10 mM AgNO$_3$ solutions, respectively. Corresponding size distribution histograms of Ag NPs are presented below each SEM image. In comparison with the Ag coating formed in 1 mM AgNO$_3$ solution, the structures presented on Fig. 3 are characterized by more dense arrangement of Ag NPs. It should promote a relatively high density of the SERS-active sites. At the same time, Ag NPs in the films deposited from the
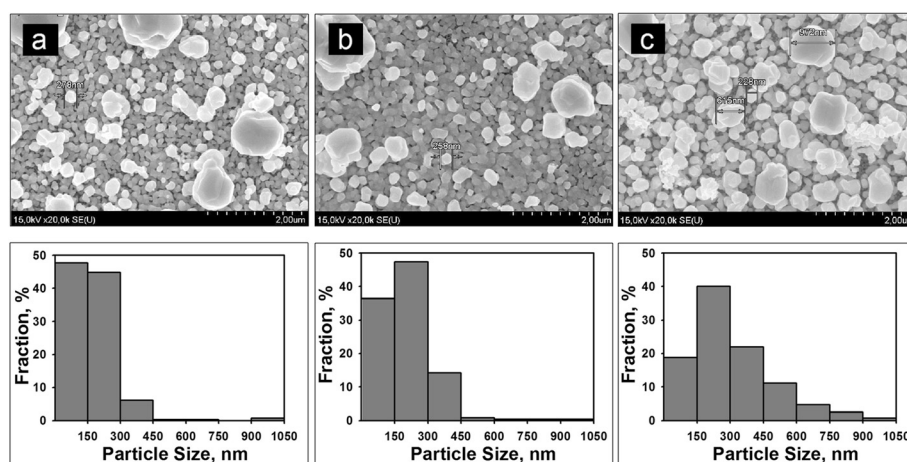

Fig. 3 SEM top views of the PS samples after the immersion into 3 mM AgNO$_3$ solution. Ag was deposited for **a** 15, **b** 120, and **c** 180 min. Below corresponding histograms of Ag NPs size distribution are presented. The histograms are normalized with respect to the total number of Ag NPs

10 mM AgNO$_3$ solution are arranged not as close to each other (Fig. 4). Hence, these Ag/PS samples are not expected to be very effective in the Raman signal enhancement.

Summarizing, there are similar regularities of the Ag deposition for all AgNO$_3$ concentrations consisting in the alternation of the following steps: the growth of the layer of the individual particles and the formation of the quasi-continuous film.

Reflectance Spectra

We characterized optical properties of the Ag/PS substrates in terms of SPR to reveal an appropriate excitation conditions for the SERS measurements. The position and intensity of SPR for the Ag nanostructures formed by the immersion deposition from the 1 mM AgNO$_3$ solution for different periods are presented on Fig. 5. The spectra show marked bands corresponding to plasmon resonances related to absorption/scattering processes of the Ag coating. For the Ag/PS samples formed during 15 and 120 min, the SPR band is rather narrow and its position is located near 390–410 nm. For the sample fabricated by the longer deposition of Ag, the SPR band is quite wide and shifted to the 550-570 nm. The intensity of the SPR band of the second sample (120 min immersion deposition) is higher than that of other samples. Indirectly, it indicates a greater SERS activity of the corresponding sample jumping together with the conclusion made after the structural study of the samples. The observed behavior of the SPR bands can be explained by the gradual increase of the Ag NPs dimensions during their growth and an effect of the interparticle plasmonic coupling [45]. It should be noticed that such kind of the Ag nanostructures has a complex multilayer morphology where multipolar surface plasmon resonances can be realized.
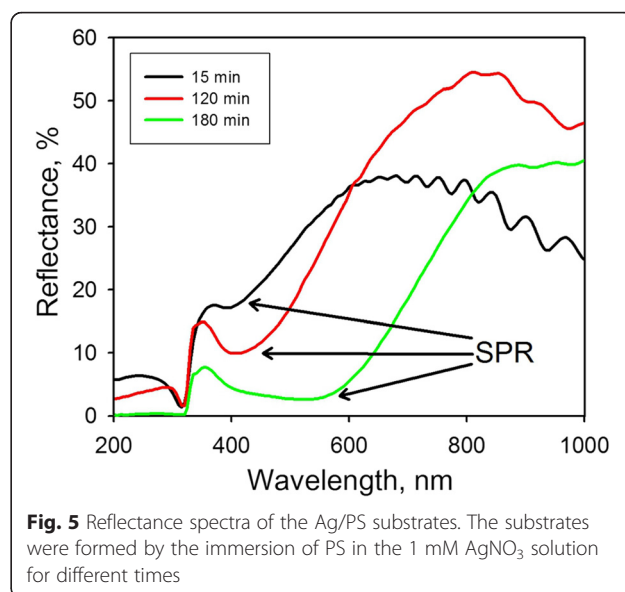

Fig. 5 Reflectance spectra of the Ag/PS substrates. The substrates were formed by the immersion of PS in the 1 mM AgNO$_3$ solution for different times

Dependence of the SERS Activity on the Ag Deposition Conditions

A comparison of the Raman spectra intensity for the CuTMpyP4 molecules adsorbed on the PS and Ag/PS substrates revealed the SERS activity of the Ag-coated samples. The typical SERS spectrum of the CuTMpyP4 shown on Fig. 6 was observed for all Ag/PS substrates studied.

Figure 7 shows the dependence of the 1366 cm^{-1} band intensity in the SERS spectrum of 10^{-6} M CuTMpyP4 on the immersion time for the samples of Ag/PS formed in 1, 3 and 10 mM AgNO$_3$ solutions. Remarkable, the graphs have two peaks of the SERS-signal intensity. For example, in case of 1 mM concentration, they are located in the intervals of 100–140 and 200–270 min. The maxima of the Raman signal for the samples formed in
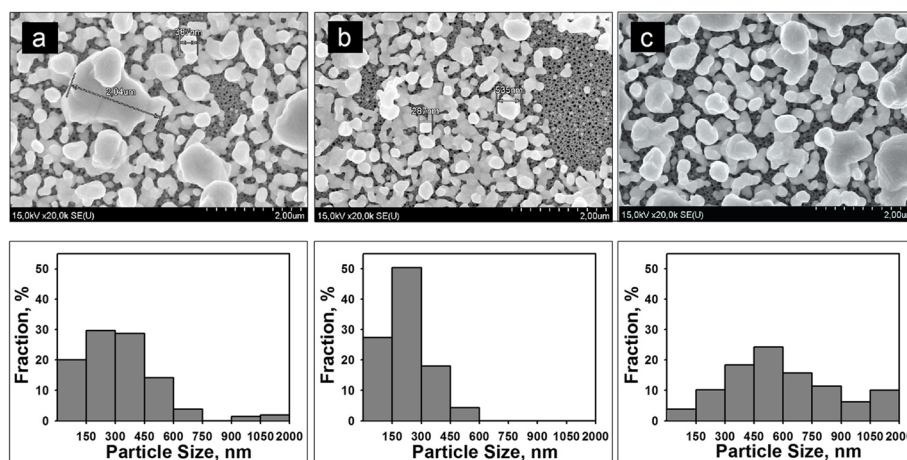

Fig. 4 SEM top views of the PS samples after the immersion into 10 mM AgNO$_3$ solution. Ag was deposited for **a** 15, **b** 120, and **c** 180 min. Below corresponding histograms of Ag NPs size distribution are presented. The histograms are normalized with respect to the total number of Ag NPs
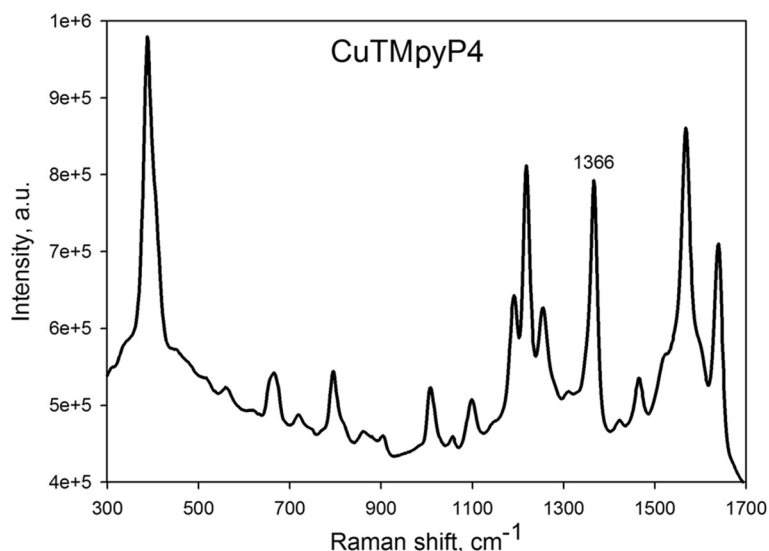
Fig. 6 SERS spectrum of the analyte molecules adsorbed on the Ag/PS substrate. A 10^{-6} M CuTMpyP4 aqueous solution was used as analyte solution. The Ag/PS substrate was formed by the immersion of PS in the 1 mM AgNO$_3$ solution for 120 min

3 mM AgNO$_3$ solution are related to the deposition during 40 and 70 min, while in the case of the 10 mM AgNO$_3$ solution, they can be found at 12–15 and 21 min. It is reasonable to suggest that the observed behavior of the SERS-signal intensity is caused by the peculiarities of the Ag film growth described before. Therefore, to propose the origin of two maxima in SERS intensity, we put together the stages of the Ag deposition and the deposition periods resulted in the greatest SERS-signal intensity. The analysis of the Fig. 2 shows that in the Ag deposition beginning (15 min), there is a long distance between Ag NPs, which

results in a low level of the Raman signal. The next morphological type of the quasi-continuous Ag film is favorable for the effective SERS due to closely packed Ag agglomerates, which promote the abundance of vacancies for the so-called hot spots, where the scattering cross section of the analyte's molecules drastically increases. This structure matches with the first peak of the SERS-signal intensity. The following decrease of the SERS signal is related to the morphology where the Ag agglomerates partially disconnected and coalesced into the larger Ag structures (Fig. 2c). Finally, the new sub-layer of the
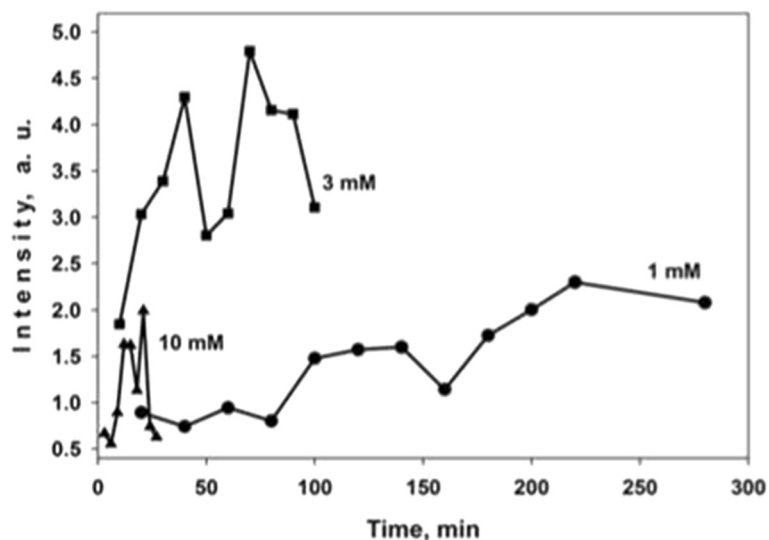

Fig. 7 Dependence of SERS-signal intensity on the time of PS immersion in 1, 3 and 10 mM AgNO$_3$ solutions. A 10^{-6} M CuTMpyP4 aqueous solution was used as analyte solution. The SERS-signal intensity of the 1366 cm^{-1} band in the SERS spectrum of 10^{-6} M CuTMpyP4 was estimated

small Ag NPs grew on the newly opened PS surface giving rise to the second maximum in the SERS-signal intensity.

The same correlation between the Ag-coating morphology and SERS-signal intensity can be found for the samples fabricated in the 3 and 10 mM $AgNO_3$ solutions.

Effective Time Parameter

Based on the performed analysis of the regularities of the Ag nanostructures growth via the Volmer–Weber mechanism and the SERS-signal intensity dependence on the Ag immersion time, we have proposed a universal parameter crucial for the choice of the optimal formation conditions of SERS-active substrates. This parameter was called an effective time (ET) and calculated as a product of the $AgNO_3$ concentration ([$AgNO_3$]) by the Ag immersion deposition time (t_{imm}):

$$ET = t_{imm} \cdot [AgNO_3]$$

Figure 8 demonstrates the dependence of the SERS-signal intensity on the effective time. For example, for the 1 mM $AgNO_3$ concentration and 100 min immersion time ET = 0.1. In fact, two distinct maxima of the SERS-signal intensity are observed for three types of the Ag/PS substrates formed at the same effective times. Taking into account the efforts in the area of a technology development of highly effective SERS-active substrates with reproducible properties, we believe that the effective time is very useful for a choice of the conditions of the Ag immersion deposition on meso-PS.

Detection Limit

One of the most adequate parameters traditionally used to characterize the SERS-active substrates is a detection limit. This parameter means a minimal concentration of analyte, which can be detected with the SERS-active substrate. In the previous section, we have demonstrated that the $AgNO_3$ concentration does not affect the order of magnitude of the SERS-signal intensity (Fig. 7). Nevertheless, the SERS-signal intensity provided by the samples formed in the 3 mM $AgNO_3$ solution is almost two times more than that of the substrates fabricated in the 1 and 10 mM $AgNO_3$
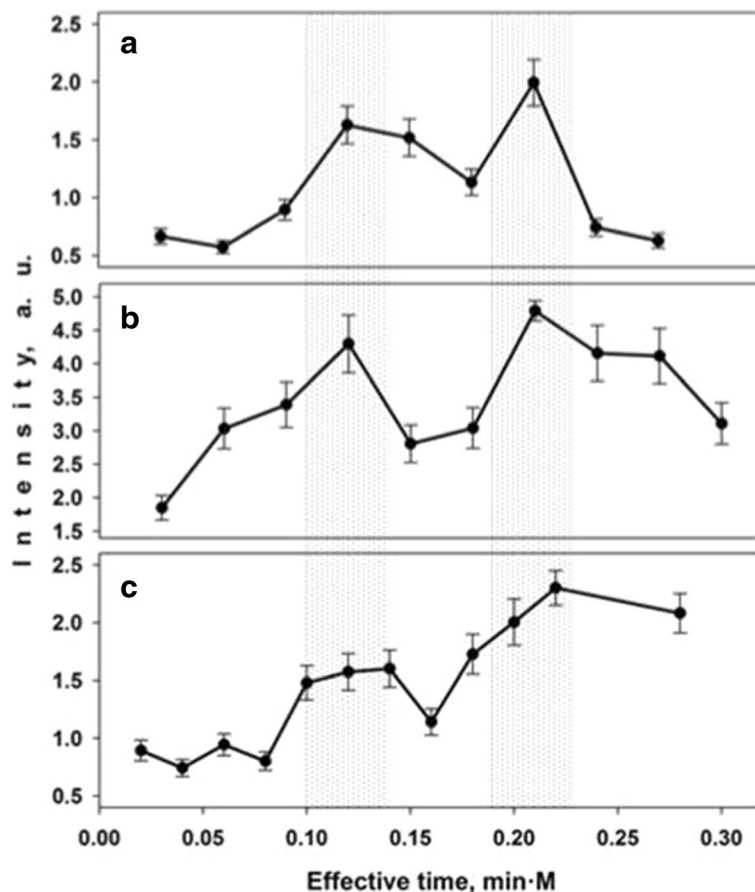

Fig. 8 Dependence of SERS-signal intensity on effective time for **a** 1, **b** 3 and **c** 10 mM $AgNO_3$ solutions. A 10^{-6} M CuTMpyP4 aqueous solution was used as analyte solution. The SERS-signal intensity of the 1366 cm^{-1} band in the SERS spectrum of 10^{-6} M CuTMpyP4 was estimated

Bandarenka *et al. Nanoscale Research Letters* (2016) 11:262

Page 9 of 11

solutions. That is why we evaluated the detection limit using the substrates prepared in the 3 mM AgNO$_3$ solution for 40 min, because exactly this immersion time provides the most intensive SERS signal. Figure 9 shows SERS spectra and the detection limit of the CuTMpyP4 molecules adsorbed on the Ag/PS substrates from the solutions with different concentrations (10^{-6}–10^{-11} M). As seen from Fig. 9, the detection limit of the Ag/PS substrates formed by the immersion deposition of silver for 40 min reaches 10^{-11} M.
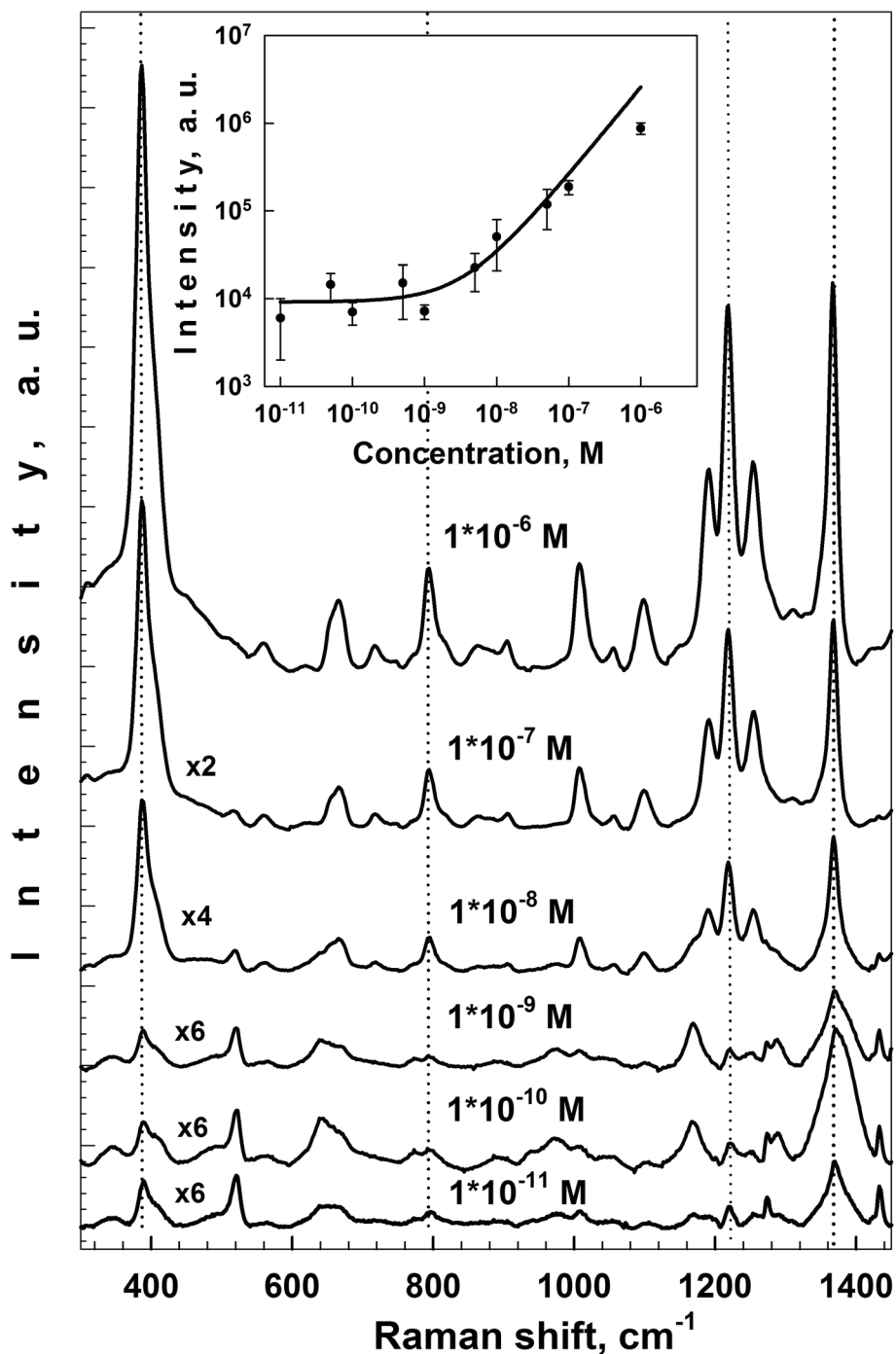

Fig. 9 SERS spectra and detection limit of the CuTMpyP4 molecules adsorbed on the Ag/PS substrates. 10^{-6}–10^{-11} M CuTMpyP4 aqueous solutions were used as analyte solutions. The Ag/PS substrates were formed by the immersion deposition of silver on PS from 3 mM AgNO$_3$ solution for 40 min

Bandarenka *et al. Nanoscale Research Letters* (2016) 11:262

Page 10 of 11

Conclusions

Plasmonic Ag nanostructures have been formed on the meso-PS by the immersion plating procedure. Morphological and optical properties of the fabricated Ag films were characterized by XRD, SEM, and UV–Vis reflectance spectroscopy. Raman enhancement has been evaluated using water-soluble cationic porphyrin CuTMPyP4. The maxima of the SERS-signal intensity were observed for the samples obtained by the PS immersion in the 3 mM $AgNO_3$ aqueous solution with ethanol additive for 40 and 70 min. The detection limit for the CuTMPyP4 molecules adsorbed on Ag/PS surface was evaluated as 10^{-11} M. The comparative analysis of the data on the morphology and SERS activity of the Ag/PS substrates allows concluding that the optimal Ag films providing the maximal Raman enhancement for the same kind of the PS substrate can be formed taking into account a specific parameter called effective time. This parameter is a product of the $AgNO_3$ concentration by the Ag immersion deposition time. The results obtained for the concentration/time relation are useful upon choice of the immersion reaction conditions for preparation SERS-active substrates based on mesoporous silicon.

Abbreviations

NPs: nanoparticles; PS: porous silicon; SEM: scanning electron microscopy; SERS: surface-enhanced Raman scattering; SPR: surface plasmon resonance; XRD: X-ray diffraction.

Competing interests

The authors declare that they have no competing interests.

Authors' contributions

HVB carried out fabrication of the Ag/PS substrates, analyzed XRD diffraction patterns, reflectance and SERS spectra, and designed and drafted the manuscript. KVG fabricated the samples, recorded reflectance spectra, analyzed SEM images, and prepared figures for the manuscript. AYuP performed adsorption of the analyte molecules on the Ag/PS substrates and explained the SERS spectra. IAK conducted SERS measurements. VPB and SNT initiated, planned, and controlled the research process. All authors read and approved the final manuscript.

Author details

[1]Laboratory of Materials and Structures of Nanoelectronics, Belarusian State University of Informatics and Radioelectronics, 6 Brovka st., Minsk 220013, Belarus. [2]B.I. Stepanov Institute of Physics of National Academy of Sciences of Belarus, 68 Nezalezhnasti av., Minsk 220072, Belarus.

References

1. Kneipp K, Kneipp H, Itzkan I, Dasari RR, Feld MS (1999) Ultrasensitive chemical analysis by raman spectroscopy. Chem Rev 99:2957–2975
2. Kim K, Shin KS (2011) Surface-enhanced Raman scattering: a powerful tool for chemical identification. Anal Sci 27:775–783
3. Kneipp J, Kneipp H, Kneipp K (2008) SERS—a single-molecule and nanoscale tool for bioanalytics. Chem Soc Rev 37:1052–1060
4. Kho KW, Fu CY, Dinish US, Olivo M (2011) Clinical SERS: are we there yet? J Biophotonics 4:667–684
5. Xie W, Schlücker S (2013) Medical applications of surface-enhanced Raman scattering. Phys Chem Chem Phys 15:5329–5344
6. Tsai YC, Hsu PC, Lin YW, Wu TM (2009) Silver nanoparticles in multiwalled carbon nanotube–Nafion for surface-enhanced Raman scattering chemical sensor. Sens Actuators B 138:5–8
7. Stoddart PR, White DJ (2009) Optical fibre SERS sensors. Sens Actuators B 138:5–8
8. Halvorson R, Vikesland PJ (2010) Surface-enhanced Raman spectroscopy (SERS) for environmental analyses. Environ Sci Technol 44:7749–7755
9. Cîntă Pînzaru S, Pavel I, Leopold N, Kiefer W (2004) Identification and characterization of pharmaceuticals using Raman and surface-enhanced Raman scattering. J Raman Spectrosc 35:338–346
10. Aroca R (2006) Surface-enhanced vibrational spectroscopy. Wiley, Chichester
11. Masuda H, Fukuda K (1995) Ordered metal nanohole arrays made by a two-step replication of honeycomb structures of anodic alumina. Science 268: 1466–1468
12. Moskovits M (1985) Surface-enhanced spectroscopy. Rev Mod Phys 57:783–826
13. Kneipp K, Moskovits M, Kneipp H (2007) Surface-enhanced Raman scattering. Phys Today 60:40–46
14. Kerker M, Wang DS, Chew H (1980) Surface enhanced Raman scattering (SERS) by molecules adsorbed at spherical particles. Appl Opt 19:3373–3388
15. Lombardi JR, Birke RL (2008) A unified approach to surface-enhanced Raman spectroscopy. J Phys Chem C 112:5605–5617
16. Brown RJ, Milton MJ (2008) Nanostructures and nanostructured substrates for surface-enhanced Raman scattering (SERS). J Raman Spectrosc 39:1313–1326
17. Fana M, Andradec GF, Brolo AG (2011) A review on the fabrication of substrates for surface enhanced Raman spectroscopy and their applications in analytical chemistry. Anal Chim Acta 693:7–25
18. Moskovits M (2005) Surface-enhanced Raman spectroscopy: a brief retrospective. J Raman Spectrosc 36:485–496
19. Baker GA, Moore DS (2005) Progress in plasmonic engineering of surface-enhanced Raman-scattering substrates toward ultra-trace analysis. Anal Bioanal Chem 382:1751–1770
20. Haynes CL, Van Duyne RP (2003) Plasmon-sampled surface-enhanced Raman excitation spectroscopy. J Phys Chem B 107:7426–7433
21. Tao A, Kim F, Hess C, Goldberger J, He R, Sun Y, Xia Y, Yang P (2003) Langmuir–Blodgett silver nanowire monolayers for molecular sensing usingsurface enhanced Raman spectroscopy. Nano Lett 3:1229–1233
22. Canham L (1997) Properties of porous silicon. INSPEC, London
23. Lazarouk S, Bondarenko V, Pershukevich P, La Monica S, Maiello G, Ferrari A. Visible electroluminescence from Al-porous silicon reverse bias diodes formed on the base of degenerate n-type silicon. Proceedings of the 1994 MRS Fall Meeting: November 28–30, 1994. Boston, MA, USA; 1995; 358:659-664.
24. Chan S, Kwon S, Koo TW, Lee LP, Berlin AA (2003) Surface-enhanced Raman scattering of small molecules from silver-coated silicon nanopores. Adv Mater 15:1595–1598
25. Giorgis F, Descrovi E, Chiodoni A, Froner E, Scarpa M, Venturello A, Geobaldo F (2008) Porous silicon as efficient surface enhanced Raman scattering (SERS) substrate. Appl Surf Sci 254:7494–7497
26. Sun X, Wang N, Li H (2013) Deep etched porous Si decorated with Au nanoparticles for surface-enhanced Raman spectroscopy (SERS). Appl Surf Sci 284:549–555
27. Huang Z, Fang H, Zhu J (2007) Fabrication of silicon nanowire arrays with controlled diameter, length, and density. Adv Mater 19:744–748
28. Chiolerio A, Virga A, Pandolfi P, Martino P, Rivolo P, Geobaldo F, Giorgis F (2012) Direct patterning of silver particles on porous silicon by inkjet printing of a silver salt via in-situ reduction. Nanoscale Res Lett 7(1):1–7
29. Lin H, Mock J, Smith D, Gao T, Sailor MJ (2004) Surface-enhanced Raman scattering from silver-plated porous silicon. J Phys Chem B 108:11654–11659
30. Virga A, Gazia R, Pallavidino L, Mandracci P, Descrovi E, Chiodoni A, Geobaldo F, Giorgis F (2010) Metal-dielectric nanostructures for amplified Raman and fluorescence spectroscopy. Phys Stat Solid C 7(3–4):1196–1199
31. Panarin AY, Chirvony VS, Kholostov KI, Turpin PY, Terekhov SN (2009) Formation of SERS-active silver structures on the surface of mesoporous silicon. J Appl Spectrosc 76:280
32. Bandarenka H, Redko S, Nenzi P, Balucani M, Bondarenko V (2012) Optimization of chemical displacement deposition of copper on porous silicon. J Nanosci Nanotechnol 12(11):8725–8731

33. Miyagawa R, Fukami K, Sakka T, Ogata YH (2011) Surface-enhanced Raman scattering from gold deposited mesoporous silicon. Phys Status Solidi A 208(6):1471–1474
34. Bandarenka H, Redko S, Smirnov A, Panarin A, Terekhov S, Nenzi P, Balucani M, Bondarenko V (2012) Nanostructures formed by displacement of porous silicon with copper: from nanoparticles to porous membranes. Nanoscale Res Lett 7:477
35. Zeiri L, Rechav K, Porat Z, Zeiri Y (2012) Silver nanoparticles deposited on porous silicon as a surface-enhanced Raman scattering (SERS) active substrate. Appl Spectrosc 66:294–299
36. Harraz FA, Ismail AA, Bouzid H, Al-Sayari SA, Al-Hajary A, Al-Assiri MS (2015) Surface-enhanced Raman scattering (SERS)-active substrates from silver plated-porous silicon for detection of crystal violet. Appl Surf Sci 331:241–247
37. Virga A, Rivolo P, Descrovi E, Chiolerio A, Digregorio G, Frascella F, Soster M, Bussolino F, Marchiò S, Geobaldo F, Giorgis F (2012) SERS active Ag nanoparticles in mesoporous silicon: detection of organic molecules and peptide–antibody assays. J Raman Spectrosc 43:730–736
38. Panarin AY, Terekhov SN, Kholostov KI, Bondarenko VP (2010) SERS-active substrates based on n-type porous silicon. Appl Surf Sci 256:6969–6976
39. Artsemyeva K, Dolgiy A, Bandarenka H, Panarin A, Khodasevich I, Terekhov S, Bondarenko V (2013) Fabrication of SERS-active substrates by electrochemical and electroless deposition of metals in macroporous silicon. ECS Transactions 53(11):85–95
40. Bandarenka H, Artsemyeva K, Redko S, Panarin A, Terekhov S, Bondarenko V (2013) Effect of swirl-like resistivity striations in n+-type Sb doped Si wafers on the properties of Ag/porous silicon SERS substrates. Phys Status Solidi C 10:624–627
41. Cardinal MF, Rodrigues-Gonzalez B, Alvarez-Puebla RA, Perez-Juste J, Liz-Marzan LM (2010) Modulation of localized surface plasmons and SERS response in gold dumbbells through silver coating. J Phys Chem 114:10417–10423
42. Balucani M, Bondarenko V, Dolgiy A, Redko SV, Bandarenka H, Prischepa SL, Yanushkevich K, Nenzi P (2012) Electrochemical deposition and characterization of Ni in mesoporous silicon. J Electrochem Soc 159(10):D623–D627
43. Oskam G, Long JG, Natarajan A, Searson PC (1998) Electrochemical deposition of metals onto silicon. J Phys D Appl Phys 31:1927–1949
44. Harraz FA, Tsuboi T, Sasano J, Sakka T, Ogata YH (2002) Metal deposition onto a porous silicon layer by immersion plating from aqueous and nonaqueous solutions. Electrochem Soc 149:456–463
45. Kreibig U, Vollmer M. Optical Properties of Metal Clusters. Berlin-Heidelberg: Springer-Verlag; 1995.